# Relativistic models for electron and neutrino-nucleus scattering

Cite as: AIP Conference Proceedings **1189**, 107 (2009); https://doi.org/10.1063/1.3274139
Published Online: 02 December 2009

C. Giusti, A. Meucci, F. D. Pacati, J. A. Caballero, and J. M. Udías



# Relativistic models for electron and neutrino-nucleus scattering

C. Giusti*, A. Meucci*, F. D. Pacati*, J. A. Caballero† and J. M. Udías**

*Dipartimento di Fisica Nucleare e Teorica, Università degli Studi di Pavia and Istituto Nazionale di Fisica Nucleare, Sezione di Pavia, I-27100 Pavia, Italy
†Departamento de Física Atómica, Molecular y Nuclear, Universidad de Sevilla, E-41080 Sevilla, Spain
**Grupo de Física Nuclear, Departamento de Física Atómica, Molecular y Nuclear, Universidad Complutense de Madrid, E-28040 Madrid, Spain

**Abstract.** Relativistic models developed for the exclusive and inclusive quasielastic (QE) electron scattering have been extended to charged-current (CC) and neutral-current (NC) neutrino-nucleus scattering. Different descriptions of final-state interactions (FSI) are compared. For the inclusive electron scattering the relativistic Green's function approach is compared with calculations based on the use of relativistic purely real mean field potentials in the final state. Both approaches lead to a redistribution of the strength but conserving the total flux. Results for the differential cross section at different energies are presented. Scaling properties are also analyzed and discussed.

**Keywords:** Relativistic models, lepton-induced reactions, electron scattering, neutrino scattering
**PACS:** 24.10.Jv, 25.30.-c, 25.30.Fj, 25.30.Pt

## INTRODUCTION

Several decades of experimental and theoretical work on electron scattering have provided a wealth of information on nuclear structure and dynamics [1]. In these experiments the electron is the probe, whose properties are clearly specified, and the nucleus the target whose properties are under investigation. Additional information on nuclear properties is available from neutrino-nucleus scattering. Neutrinos can excite nuclear modes unaccessible in electron scattering, can give information on the hadronic weak current and on the strange form factors of the nucleon. Although of great interest, such studies are not the only aim of many neutrino experiments, which are better aimed at a precise determination of neutrino properties. In neutrino oscillation experiments nuclei are used to detect neutrinos and a proper analysis of data requires that the nuclear response to neutrino interactions is well under control and the unavoidable theoretical uncertainties on nuclear effects are reduced as much as possible.

In recent years different models developed and successfully tested in comparison with electron scattering data have been extended to neutrino-nucleus scattering. Although the two situations are different, electron scattering is the best available guide to determine the prediction power of a nuclear model. Nonrelativistic and relativistic models have been developed to describe nuclear effects with different approximations. They can be considered as alternative models, but only a relativistic approach is able to account for all the effects of relativity in a complete and consistent way. Relativity is important at all energies, in particular at high energies, and in the energy regime of many neutrino experiments a relativistic approach is required.

Relativistic models for the exclusive and inclusive electron and neutrino scattering in the QE region are presented in this contribution. In the QE region the nuclear response is dominated by one-nucleon knockout processes, where the probe interacts with a quasifree nucleon that is emitted from the nucleus with a direct one-step mechanism and the remaining nucleons are spectators. In electron scattering experiments the outgoing nucleon can be detected in coincidence with the scattered electron. In the exclusive $(e,e'p)$ reaction the residual nucleus is left in a specific discrete eigenstate and the final state is completely specified. In the inclusive $(e,e')$ scattering the outgoing nucleon is not detected and the cross section includes all the available final nuclear states.

For an incident neutrino (antineutrino) NC and CC scattering can be considered

$$\begin{aligned} \nu(\bar{\nu}) + A &\rightarrow \nu'(\bar{\nu}') + N + (A-1) && \text{NC} \\ \nu(\bar{\nu}) + A &\rightarrow l^-(l^+) + p(n) + (A-1). && \text{CC} \end{aligned}$$

CP1189, *From Sixth International Workshop on Neutrino-Nucleus Interactions in the Few-GeV Region*, edited by F. Sanchez, M. Sorel, L. Alvarez-Ruso, A. Cervera, and M. Vicente-Vacas

In NC scattering only the emitted nucleon can be detected and the cross section is integrated over the energy and angle of the final lepton. Also the state of the residual $(A-1)$-nucleus is not determined and the cross section is summed over all the available final states. The same situation occurs for the CC reaction if only the outgoing nucleon is detected. The cross sections are therefore semi-inclusive in the hadronic sector and inclusive in the leptonic one and can be treated as an $(e,e'p)$ reaction where only the outgoing proton is detected. The exclusive CC process where the charged final lepton is detected in coincidence with the emitted nucleon can be considered as well. The inclusive CC scattering where only the charged lepton is detected can be treated with the same models used for the inclusive $(e,e')$ reaction.

For all these processes the cross section is obtained in the one-boson exchange approximation from the contraction between the lepton tensor, that depends only on the lepton kinematics, and the hadron tensor $W^{\mu\nu}$, that contains the nuclear response and whose components are given by bilinear products of the matrix elements of the nuclear current $J^{\mu}$ between the initial and final nuclear states, i.e.,

$$W^{\mu\nu} = \sum_{f} \langle \Psi_f \mid J^{\mu}(\mathbf{q}) \mid \Psi_i \rangle \langle \Psi_i \mid J^{\nu\dagger}(\mathbf{q}) \mid \Psi_f \rangle \, \delta(E_i + \omega - E_f), \tag{1}$$

where $\omega$ and $\mathbf{q}$ are the energy and momentum transfer, respectively. Different but consistent models to calculate $W^{\mu\nu}$ in QE electron and neutrino-nucleus scattering are outlined in the next sections.

## EXCLUSIVE ONE-NUCLEON KNOCKOUT

Models based on the relativistic distorted-wave impulse approximation (RDWIA) have been developed [2–6] to describe the exclusive reaction where the outgoing nucleon is detected in coincidence with the scattered lepton and the residual nucleus is left in a discrete eigenstate $n$. In RDWIA the amplitudes of Eq. 1 are obtained in a one-body representation as

$$\langle \chi^{(-)} \mid j^{\mu}(\mathbf{q}) \mid \varphi_n \rangle \, , \tag{2}$$

where $\chi^{(-)}$ is the single- particle (s.p.) scattering state of the emitted nucleon, $\varphi_n$ the overlap between the ground state of the target and the final state $n$, i.e., a s.p. bound state, and $j^{\mu}$ the one-body nuclear current. In the model the s.p. bound and scattering states are consistently derived as eigenfunctions of a Feshbach-type optical potential [1, 2]. Phenomenological ingredients are adopted in the calculations. The bound states are Dirac-Hartree solutions of a Lagrangian, containing scalar and vector potentials, obtained in the framework of the relativistic mean-field theory [7–9]. The scattering state is calculated solving the Dirac equation with relativistic energy-dependent complex optical potentials [10, 11]. RDWIA models have been quite successful in describing a large amount of data for the exclusive $(e,e'p)$ reaction [1–6]. The RDWIA cross sections are in excellent accordance with data. Moreover, comparison with separate response functions and asymmetries has also proved the capability of the relativistic approaches to successfully describe fine details of data behavior.

## SEMI-INCLUSIVE NEUTRINO-NUCLEUS SCATTERING

The transition amplitudes of the NC and CC processes where only the outgoing nucleon is detected are described as the sum of the RDWIA amplitudes in Eq. 2 over the states $n$. In the calculations [12–14] a pure shell-model (SM) description is assumed, i.e., $n$ is a one-hole state and the sum is over all the occupied SM states. FSI are described by a complex optical potential whose imaginary part gives an absorption that reduces the calculated cross section. The imaginary part accounts for the flux lost in a specific channel towards other channels. This approach is conceptually correct for an exclusive reaction, where only one channel contributes, but it would be wrong for the inclusive scattering, where all the channels contribute and the total flux must be conserved. For the semi-inclusive process where an emitted nucleon is detected, some of the reaction channels which are responsible for the imaginary part of the potential, like fragmentation of the nucleus, re-absorption, etc., are not included in the experimental cross section and, from this point of view, it is correct to perform calculations with the absorptive imaginary part of the optical potential. There are, however, contributions that are not included in this model and that can be included in the experimental cross section, for instance, contributions due to multi-step processes, where the outgoing nucleon is re-emitted after re-scattering in a detected channel simulating the kinematics of a QE reaction. The relevance of these contributions depends on kinematics and should not be too large in the QE region. The same uncertainties are also present in other semi-inclusive reactions, as for instance, in the analysis of the $(e,e'p)$ reaction at the QE peak, when the emission from

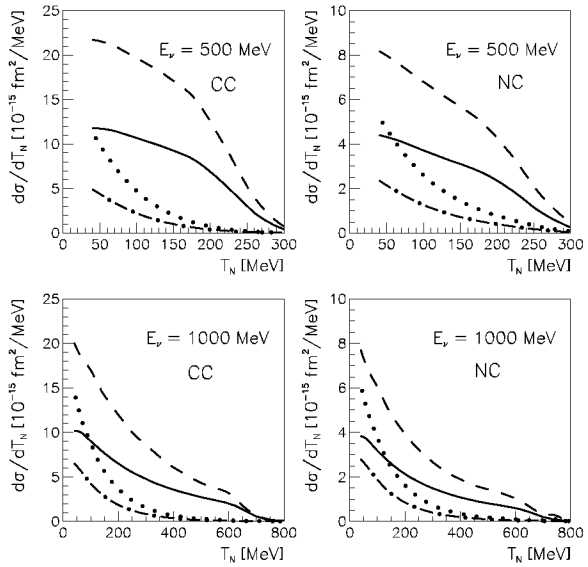


**FIGURE 1.** Differential cross sections of the CC and NC $\nu_\mu$ ($\bar{\nu}_\mu$) QE scattering on $^{12}$C as a function of $T_N$. Solid and dashed lines are the results in RDWIA and RPWIA, respectively, for an incident neutrino. Dot-dashed and dotted lines are the results in RDWIA and RPWIA, respectively, for an incident antineutrino.

deep states is considered. In this case rescattering contributions mainly affect the cross section at large angles of the emitted proton, but they are much lower than the direct contribution for missing energies less than 80 MeV and after integration over the angles [15–19].

In Figure 1 the cross sections of the $^{12}\mathrm{C}(\nu_\mu,\mu^- p)$ and $^{12}\mathrm{C}(\bar{\nu}_\mu,\mu^+ n)$ CC reactions and of the $^{12}\mathrm{C}(\nu_\mu,\nu_\mu p)$ and $^{12}\mathrm{C}(\bar{\nu}_\mu,\bar{\nu}_\mu p)$ NC reactions are compared in RPWIA and RDWIA at $E_{\nu(\bar{\nu})} = 500$ and 1000 MeV. FSI reduce the cross sections of $\simeq 50\%$. The reduction is due to the imaginary part of the optical potential and it is in agreement with the reduction found in $(e,e'p)$ calculations. We note that the cross sections for an incident neutrino are larger than for an incident antineutrino and for NC lower than for CC scattering.

## INCLUSIVE LEPTON-NUCLEUS SCATTERING

In the inclusive scattering where only the outgoing lepton is detected FSI are treated in the Green's function (GF) approach [20–23]. In this model the components of the hadron tensor are written in terms of the s.p. optical model Green's function. This is the result of suitable approximations, such as the assumption of a one-body current and subtler approximations related to the IA. The explicit calculation of the s.p. Green's function is avoided by its spectral representation, which is based on a biorthogonal expansion in terms of a non Hermitian optical potential $\mathscr{H}$ and of its Hermitian conjugate $\mathscr{H}^\dagger$. Calculations require matrix elements of the same type as the RDWIA ones in Eq. 2, but involve eigenfunctions of both $\mathscr{H}$ and $\mathscr{H}^\dagger$, where the different sign of the imaginary part gives in one case an absorption and in the other case a gain of flux. Thus, in the sum over $n$ the total flux is redistributed and conserved. The GF approach guarantees a consistent treatment of FSI in the exclusive and in the inclusive scattering and gives a good description of $(e,e')$ data [20].

In Fig. 2 the $^{16}\mathrm{O}(\nu_\mu,\mu^-)$ cross sections calculated with the GF approach are compared with the results of the relativistic plane wave IA (RPWIA), where FSI are neglected. The cross sections obtained when only the real part of the relativistic optical potential (rROP) is retained and the imaginary part is neglected are also shown in the figure. This approximation conserves the flux, but it is conceptually wrong because the optical potential has to be complex owing to the presence of inelastic channels. The partial contribution given by the sum of all the integrated exclusive one-nucleon knockout reactions, also shown in the figure, is much smaller than the complete result. The difference is

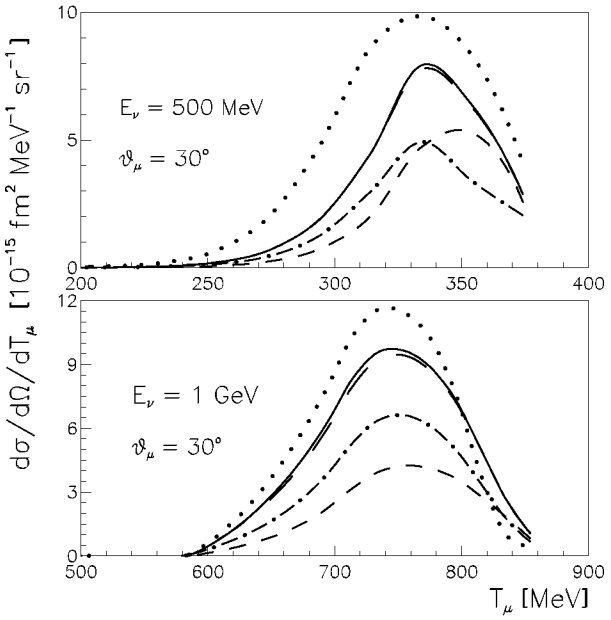


**FIGURE 2.** The cross sections of the $^{16}O(\nu_\mu, \mu^-)$ reaction for $E_\nu$ = 500 and 1000 MeV at $\theta_\mu = 30^o$ as a function of the muon kinetic energy $T_\mu$. Results for GF (solid), RPWIA (dotted), and rROP (long-dashed) are compared. The dot-dashed lines give the contribution of the integrated exclusive reactions with one-nucleon emission. Short dashed lines give the GF results for the $^{16}O(\bar{\nu}_\mu, \mu^+)$ reaction.

due to the spurious loss of flux produced by the absorptive imaginary part of the optical potential.

The analysis of data for neutrino experiments requires a precise knowledge of lepton-nucleus cross sections, where uncertainties on nuclear effects are reduced as much as possible. To this aim, it is important to check the consistency of different models and the validity of the adopted approximations.

The results of the relativistic models developed by the Pavia and the Madrid-Sevilla groups for the inclusive electron scattering are compared in [27]. As a first step the consistency of the RPWIA and rROP calculations performed by the two groups with independent numerical programs has been checked. Then the results of different descriptions of FSI have been compared. An example is shown in Fig. 3 for the $^{12}C(e,e')$ cross sections calculated with RPWIA, rROP, GF with two parametrizations of the optical potential [10], i.e., EDAD1 (GF1) and EDA2 (GF2), and the relativistic mean field (RMF) [28], where the scattering wave functions are calculated with the same real potential used for the initial bound states. The RMF model fulfills the dispersion relation and maintains the continuity equation. The differences between RMF and GF increase with $q$: they are small at $q$ = 500 MeV/$c$ and significant at $q$ = 1000 MeV/$c$. The RMF cross section shows an asymmetry, with a long tail extending towards higher values of $\omega$. A less significant asymmetry is obtained for both GF1 and GF2 cross sections, that at $q$ = 1000 MeV/$c$ are higher than the RMF one in the maximum region. The enhancement is different for the two optical potentials. The behaviour of the RMF and GF results as a function of $q$ and $\omega$ is linked to the structure of the relativistic potentials involved in the RMF and GF models. Whereas RMF is based on the use of a strong energy-independent real potential, GF makes use of a complex energy-dependent optical potential. In GF calculations the behavior of the optical potential changes with the momentum and energy transferred in the process, and higher values of $q$ and $\omega$ correspond to higher energies for the optical potential. The GF results are consistent with the general behavior of the optical potentials and are basically due to their imaginary part, that includes the overall effect of the inelastic channels and is not univocally determined by the elastic phenomenology. Different parameterizations give similar real terms and the rROP cross sections are practically insensitive to the choice of the optical potential. The real part decreases increasing the energy and the rROP result approaches the RPWIA one for large values of $\omega$. In contrast, the imaginary part has its maximum strength around 500 MeV and is sensitive to the parameterization of the ROP. The imaginary part gives large differences between GF and rROP in Fig. 3, while only negligible differences are obtained in the different situation and kinematics of Fig. 2.

In Fig. 4 the GF1, GF2, and RMF results are compared with the experimental cross sections for three different

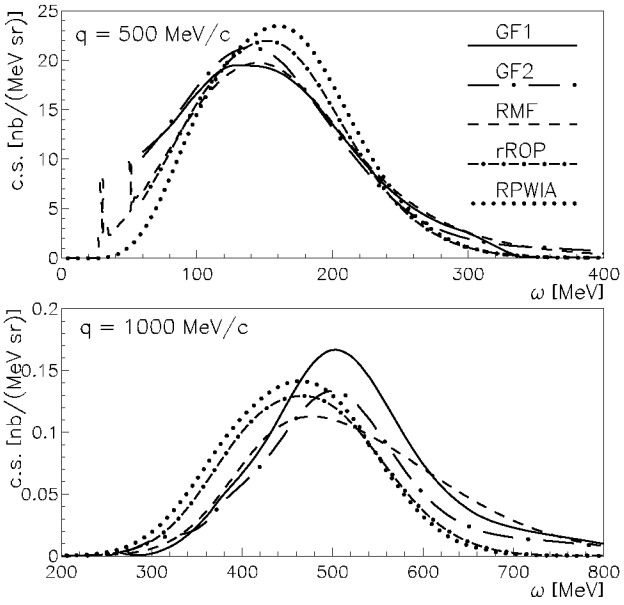


**FIGURE 3.** The cross sections of the $^{12}$C$(e,e')$ reaction for an incident electron energy of 1 GeV, $q$ = 500 (top panel) and 1000 MeV/$c$ (bottom panel), with RPWIA (dotted), rROP (dot-dashed), RMF (dashed), and GF with two optical potentials, EDAD1 (GF1 solid) and EDA2 (GF2 long dot-dashed) [10].

kinematics. The three models lead to similar cross sections. The main differences are presented for higher values of $q$, about 800 MeV/$c$ (bottom panel), where the GF1 cross section is larger than the GF2 and RMF ones. The experimental cross section is slightly underpredicted in the top panel and well described in the middle panel by all calculations. The results in the bottom panel show a fair agreement with data for GF1, whereas GF2 and RMF underpredict the experiment. Although satisfactory on general grounds, the comparison with data gives here only an indication and cannot be conclusive until contributions beyond the QE peak, like meson exchange currents and $\Delta$ effects, which may play a significant role in the analysis of data even at the maximum of the QE peak, are carefully evaluated [29–31].

## SCALING FUNCTIONS

The comparison between the results of the Pavia and Madrid-Sevilla groups has been extended to the analysis of the scaling properties of the different relativistic models [27].

Scaling ideas applied to inclusive QE electron-nucleus scattering have been shown to work properly to high accuracy [32–34]. At sufficiently high momentum transfer a scaling function is derived dividing the experimental $(e,e')$ cross sections by an appropriate single-nucleon cross section. This is basically the idea of the IA. If this scaling function depends only upon one kinematical variable, the scaling variable, one has scaling of first kind. If the scaling function is roughly the same for all nuclei, one has scaling of second kind. When both kinds of scaling are fulfilled, one says that superscaling occurs. An extensive analysis of electron scattering data has shown that scaling of first kind is fulfilled at the left of the QE peak and broken at its right, whereas scaling of second kind is well satisfied at the left of the peak and not so badly violated at its right. A phenomenological scaling function $f_L^{exp}(\psi')$ has been extracted from data of the longitudinal response in the QE region. The dimensioneless scaling variable $\psi'(q,\omega)$ is extracted from the relativistic Fermi gas (RFG) analysis that incorporates the typical momentum scale for the selected nucleus [32, 35]. Although many models based on the IA exhibit superscaling, even perfectly as the RFG, only a few of them are able to reproduce the asymmetric shape of $f_L^{exp}(\psi')$ with a significant tail extended to high values of $\omega$ (large positive values of $\psi'$). One of these is the RMF model where FSI are described by the same real relativistic potential used for the initial bound states. In contrast, the RPWIA and rROP, although satisfying superscaling properties, lead to symmetrical-shape scaling functions which are not in accordance with data analysis [35, 36].

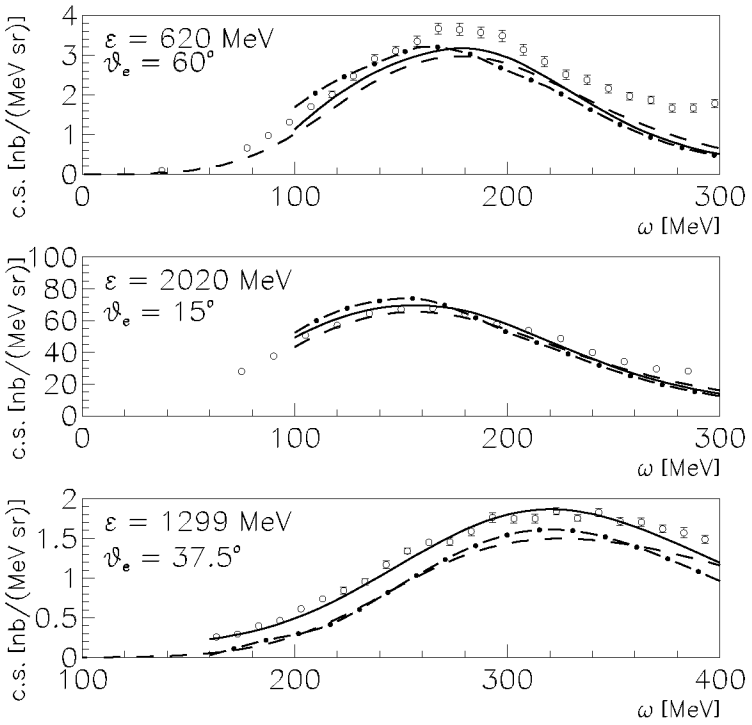


**FIGURE 4.** Differential cross section of the $^{12}$C$(e,e')$ reaction for different beam energies and electron scattering angles. Line convention: GF1 (solid), GF2 (dot-dashed), and RMF (dashed). Experimental data from [24–26].

In Fig. 5 the scaling function $f_L(\psi')$ evaluated with RMF, GF1, and GF2 for different values of $q$ are compared to the phenomenological function $f_L^{exp}(\psi')$. The RMF model produces an asymmetric shape with a long tail in the region with $\psi' > 0$ that follows closely the phenomenological function behavior. The GF results are similar to the RMF ones at $q$ = 500 MeV/$c$ and, with moderate differences, at $q$ = 800 MeV/$c$, while visible discrepancies appear at $q$ = 1000 MeV/$c$. The discussion of the results is similar to the one applied to the cross sections in Fig. 4, i.e., at higher $q$-values the maximum strength occurs for GF1 being RMF the weakest. The asymmetric shape with a tail in the region of positive $\psi'$ is obtained in both RMF and GF. The different dependence on $q$ shown by the potentials involved in RMF and GF makes the tail of the GF scaling function less pronounced as the value of $q$ goes up.

Except for the highest value of $q$ considered (1000 MeV/$c$), GF1, GF2 and RMF yield very similar predictions for $f_L(\psi')$, in good agreement with the experimental function. The asymmetric tail of the data and the strength at the peak are fairly reproduced by the three approaches. For $q$ = 1000 MeV/$c$, however, only RMF seems to be favoured from the comparison to data, while GF1 and GF2 yield now rather different predictions than RMF, that seem to be ruled out by data. We note that as the momentum transfer increases the phenomenological optical potentials, that is used as input in the GF approach, will (implicitely) incorporate a larger amount of contributions from non nucleonic degrees of freedom, such as, for instance, the loss of (elastic) flux into the inelastic $\Delta$ excitation with or without real pion production. Thus the input of the GF formalism is contaminated by non purely nucleonic contributions. As a consequence, GF predictions depart from the experimental QE longitudinal response, that effectively isolates only nucleonic contributions. This difference, which increases with increasing $q$, emerges as an excess of strength predicted by the GF model as it translates a loss of flux due to non-nucleonic processes into inclusive purely nucleonic strength. On the other hand, the RMF model uses as input the effective mean field that reproduces saturation properties of nuclear matter and of the ground state of the nuclei involved, and thus it is more suited to estimate the purely nucleonic contribution to the inclusive cross-section, even at $q$ = 1000 MeV/$c$.

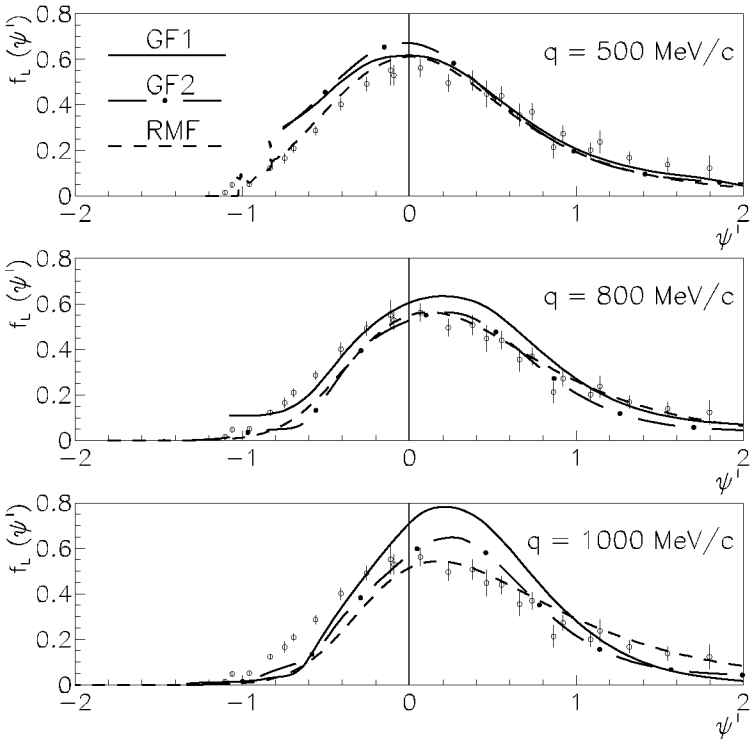


**FIGURE 5.** Longitudinal contribution to the scaling function for $q = 500$, 800, and 1000 MeV/$c$ with the GF1 (solid), GF2 (long dot-dashed), and RMF (dashed) models compared with the averaged experimental scaling function.

## SUMMARY AND CONCLUSIONS

Relativistic models developed for QE electron scattering and successfully tested in comparison with data have been extended to calculate CC and NC neutrino-nucleus cross sections. In the models nuclear effects are treated consistently in exclusive, semi-inclusive and inclusive reactions. Numerical predictions can be given for different nuclei and kinematics.

The comparison of the numerical results of different models is important to reduce theoretical uncertaintied on nuclear effects. The results of the relativistic models developed by the Pavia and the Madrid-Sevilla groups to describe FSI in the inclusive QE electron-nucleus scattering have been compared. The consistency of the calculations of the two groups has been checked in RPWIA and rROP. Then two different models based on the RIA have been compared: the GF approach of the Pavia group, that is based on the use of the complex relativistic optical potential and which allows one to treat FSI consistently in the inclusive and exclusive reactions, and the RMF model of the Madrid-Sevilla group, where the distorted waves are obtained with the same real relativistic mean field considered for the bound states. Results are compared for the differential cross sections and scaling functions. Discrepancies increase with the momentum transfer. This is linked to the energy-dependent optical potentials involved in the GF method by contrast to the energy-independent RMF potentials. Moreover, results presented for two different parameterizations of the optical potential prove the importance of the imaginary term, which gets its maximum strength around 500 MeV, whereas the real part gets smaller as the energy increases.

All models considered respect scaling and superscaling properties. The significant asymmetry in the scaling function produced by the RMF model is strongly supported by data [35]. The relativistic GF approach leads to similar results to RMF, i.e., with the asymmetry for intermediate $q$-values. Visible discrepancies, however, emerge for larger $q$, being the GF scaling function tail less pronounced but showing more strength in the region where the maximum occurs. Moreover, the GF results for high $q$ present a strong dependence on the specific parameterization of the optical potential, in particular of its imaginary part. The relativistic GF approach, even based on the use of a complex optical

potential, preserves flux conservation and the imaginary term leads to a redistribution of the strength among different channels. This explains the difference observed between RMF and GF predictions, the latter with additional strength in the region close to the maximum in the QE response. This behavior could be connected with effects coming from the contribution of the $\Delta$ which are, somehow, accounted for in a phenomenological way by the GF approach, modifying the responses even in the region where the QE peak gives the main contribution. We must keep in mind that the higher the momentum transfer, the stronger the overlap between the QE and $\Delta$ peaks, and it is very difficult to isolate contributions coming from either region.

The present analysis can be helpful to disentangle different treatments of FSI and their connections with different aspects involved in the process. The similarities of the GF and RMF predictions, particularly for intermediate values of $q$, in spite of the different phenomenological ingredients they consider, and the very reasonable agreement with the data for the longitudinal scaled response, that constitutes a good representation of the experimentally measured purely nucleonic response to the inclusive cross-sections, are a clear indication that both models make a very decent job in estimating the inclusive contribution.

## REFERENCES


1. S. Boffi, C. Giusti, F. D. Pacati, and M. Radici, *Electromagnetic Response of Atomic Nuclei*, Oxford University Press, 1996.
2. A. Meucci, C. Giusti, and F. D. Pacati, *Phys. Rev. C* **64**, 014604 (2001).
3. A. Meucci, C. Giusti, and F. D. Pacati, *Phys. Rev. C* **64**, 064615 (2001).
4. J. M. Udías et al., *Phys. Rev. C* **48**, 2731 (1993).
5. J. M. Udías et al., *Phys. Rev. C* **51**, 3246 (1995).
6. J. M. Udías et al., *Phys. Rev. C* **64**, 024614 (2001).
7. W. Pöschl, D. Vretenar, and P. Ring, *Comp. Phys. Commun.* **103**, 217 (1997).
8. G. A. Lalazissis, J. König, and P. Ring, *Phys. Rev. C* **55**, 540 (1997).
9. M. M. Sharma, M. A. Nagarajan, and P. Ring, *Phys. Lett. B* **312**, 377 (1993).
10. B. C. Clark, *Proc. of the Workshop on Relativistic Dynamics and Quark-Nuclear Physics*, edited by M. B. Johnson and A. Picklesimer, John Wiley & Sons,, New York, 1986, p. 302.
11. E. D. Cooper et al., *Phys. Rev. C* **47**, 297 (1993).
12. A. Meucci, C. Giusti, and F. D. Pacati, *Nucl. Phys. A* **744**, 307 (2004).
13. A. Meucci, C. Giusti, and F. D. Pacati, *Nucl. Phys. A* **773**, 250 (2006).
14. A. Meucci, C. Giusti, and F. D. Pacati, *Acta. Phys. Polonica B* **37**, 2279 (2006).
15. G. P. Capitani et al., *Nuovo Cimento* **85**, 37 (1985).
16. T. Takaki, *Phys. Rev. C* **39**, 359 (1989).
17. P. Demetriou, S. Boffi, C. Giusti, and F. D. Pacati, *Nucl. Phys. A* **625**, 57 (1997).
18. P. Demetriou, S. Boffi, C. Giusti, and F. D. Pacati, *Nucl. Phys. A* **634**, 513 (1998).
19. P. Demetriou et al., *Nucl. Phys. A* **650**, 199 (1999).
20. A. Meucci, F. Capuzzi, C. Giusti, and F. D. Pacati, *Phys. Rev. C* **67**, 054601 (2003).
21. A. Meucci, C. Giusti, and F. D. Pacati, *Nucl. Phys. A* **739**, 277 (2004).
22. F. Capuzzi, C. Giusti, and F. D. Pacati, *Nucl. Phys. A* **524**, 681 (1991).
23. A. Meucci, C. Giusti, and F. D. Pacati, *Nucl. Phys. A* **756**, 359 (2005).
24. P. Barreau et al., *Nucl. Phys. A* **402**, 515 (1983).
25. D. B. Day et al., *Phys. Rev. C* **48**, 1849 (1993).
26. R. Sealock et al., *Phys. Rev. Lett.* **62**, 1350 (1989).
27. A. Meucci et al., *Phys. Rev. C* **80**, 024605 (2009).
28. J. A. Caballero et al., *Phys. Rev. Lett.* **95**, 252502 (2005).
29. M. B. Barbaro, J. A. Caballero, T. W. Donnelly, and C. Maieron, *Phys. Rev. C* **69**, 035502 (2004).
30. J. E. Amaro et al., *Phys. Rev. C* **71**, 015501 (2005).
31. M. V. Ivanov et al., *Phys. Rev. C* **77**, 034612 (2008).
32. C. Maieron, T. W. Donnelly, and I. Sick, *Phys. Rev. C* **65**, 025502 (2002).
33. T. W. Donnelly, and I. Sick, *Phys. Rev. Lett.* **82**, 3212 (1999).
34. T. W. Donnelly, and I. Sick, *Phys. Rev. C* **60**, 065502 (1999).
35. J. A. Caballero, *Phys. Rev. C* **74**, 015502 (2006).
36. J. A. Caballero et al., *Phys. Rev. Lett.* **95**, 252502 (2005).